

Multiple scattering approach to elastic low-energy electron collisions with the water dimer

D. Bouchiha, L. G. Caron[†], J. D. Gorfinkiel* and L. Sanche

Groupe en Science des Radiations, Département de Médecine Nucléaire et Radiobiologie,
Faculté de Médecine, Université de Sherbrooke, Sherbrooke, Qc, J1H 5N4 Canada

*Department of Physics and Astronomy, The Open University, Walton Hall, MK7 6AA
Milton Keynes, UK

[†]Département de Physique et Regroupement Québécois sur les Matériaux de Pointe,
Université de Sherbrooke, Sherbrooke, Qc, J1K 2R1 Canada

Abstract. Multiple scattering theory is applied to low-energy electron collisions with a complex target formed of two molecular scatterers. The total T-matrix is expressed in terms of the T-matrix for each isolated molecule. We apply the approach to elastic electron-(H₂O)₂ collisions. Following the method developed in our previous work on crystalline ice (Caron et al. 2007), we impose a cut-off on the dipole outside the R-matrix sphere and an energy dependent cut-off on the angular momentum components of the monomer T-matrix. An R-matrix calculation of electron-dimer collisions is performed in order to evaluate the accuracy of the multiple scattering approach. The agreement between the two calculations is very good.

PACS numbers: 34.10.+x, 34.80.Bm, 36.40.-c

1. Introduction

In biological systems, water is present in a wide range of environments. As a highly polar molecule, water tends to trap low-energy electrons (LEEs) and is expected to play an important role in LEE-induced processes (Garrett et al. 2005, Ptasinska & Sanche 2007). Electron collisions with water vapour being the simplest to study, extensive experimental (Lozier 1930, Schulz 1960, Compton & Christophorou 1967, Sanche & Schulz 1972, Belic et al. 1981, Curtis & Walker 1992, Fedor et al. 2006, Rawat et al. 2007) and theoretical (Gil et al. 1994, Morgan 1998, Gorfinkiel et al. 2002, Haxton et al. 2007) work has been carried out (for a comprehensive review of work on electron scattering from gas phase water up to 2004 see Itikawa & Mason 2005). In the more complicated condensed phase systems, experimental studies of electron scattering from amorphous solid water, porous amorphous solid water and crystalline ice have been reported (Rowntree et al. 1991, Simpson et al. 1997, Michaud et al. 2003, Herring-Captain et al. 2005). In water clusters, formation of (H₂O)_n⁻ by attachment of slow electrons has also been investigated (Knapp et al. 1986, Knapp et al. 1987, Weber et al. 1999, Barnett et al. 1989, Lee et al. 1991) in order to elucidate the mechanism of electron solvation. To our knowledge, no theoretical investigation of electron scattering with clusters or condensed water have been reported; available methods are mainly developed for

electron collisions with gas-phase molecules. It is therefore highly desirable to develop a new theoretical approach for condensed-matter and cluster environments especially since many electron-driven processes occur in these media.

The main idea behind the multiple scattering (MS) method is to separate the potential of a complex target into non-overlapping regions with each region taken as a single scatterer. The impinging wave on each scatterer is composed of the incident plane wave and the wave scattered from the other scattering centres. The advantage of such an approach is that one can determine the cross section for large systems by combining information from its subunits. This enables the study of larger targets (macromolecules, molecular clusters, etc.) than is possible using the methods currently available.

The MS approach to LEE scattering was previously proposed by two of the authors (L. Caron and L. Sanche) (Caron & Sanche 2003, Caron & Sanche 2004, Caron & Sanche 2005) and its use in conjunction with R-matrix calculations was recently validated (Caron et al. 2007) (hereafter referred to as I). The proposed approach combines scattering gas-phase data, obtained from accurate *ab initio* R-matrix calculations, to derive scattering information for a condensed-matter situation. The partitioning of the space in the R-matrix method makes it ideal for a multiple scattering approach of the "muffin-tin" type. The method is forcibly less rigorous than the ones available for small gas-phase targets, but it is fast and, for the systems tested so far, yields very good results.

In I, we have used the MS theory in the condensed phase, using the equivalent KKR (Korringa, Kohn, and Rostoker) approach, in combination with gas-phase R-matrix data in the form of T-matrices. We were able to derive the band structure of a molecular crystal (ice). The present work constitutes a first attempt to determine elastic cross section (CS) for LEE scattering from a molecular cluster using the MS approach. The water dimer is an excellent choice for such an attempt, primarily because, making use of our previous experience in electron-H₂O collisions (Gorfinkiel et al. 2002), we were able to perform accurate R-matrix calculations of electron-dimer collisions and test the MS technique. In addition, water is present in a large variety of environments and information on LEE interactions with it is highly relevant. For example, the characteristics of the water in some of the solvation layers surrounding the double-helix structure of DNA are not that of bulk water (Becker et al. 1997), so may be explained in terms of clustered H₂O.

The main question we address in this paper is whether a multiple scattering approach is a good alternative to the computationally heavy *ab initio* methods for large to very large targets. For this purpose, we investigate how to apply the cut-offs found in I in order to perform a MS calculation of LEE collision with the water dimer.

2. Theory

In this section we present a multiple scattering method to calculate the total T-matrix, \mathbf{T}^{tot} , describing LEE collisions from a target consisting of two identical scatterers from their individual T-matrices \mathbf{T} . The monomers, labelled with the index n , are located at $\vec{R}_n = \vec{R}_\pm = \pm \vec{R}$.

The asymptotic wave function far away from the centre of mass of the two molecules can be expressed as follows:

$$\psi(\vec{r}) = \sum_{LL'} Y_{L'}(\hat{r}) \left[j_{L'}(\kappa r) \delta_{LL'} + \frac{1}{2} h_{L'}^{(+)}(\kappa r) T_{L'L}^{tot} \right] f_L^0. \quad (1)$$

where r is the relative coordinate of the scattered electron and the centre of mass of the target. The Y_L are spherical harmonics with $L = (l, m)$, j_l denotes the spherical Bessel functions and $h_l^{(+)}$ the spherical Hankel functions of the first kind. $\kappa = \sqrt{E}$ with E the energy of the incoming electron and f_L^0 is an amplitude factor for the incident plane wave. The first term on the right side of (1) corresponds to the total incident wave and the second to the total scattered wave.

We need to re-expand the incident wave in (1) around the centre of mass of each scatterer n . We use the general re-expansion formula from Dill & Dehmer (1974) which, for the spherical harmonics defined by Messiah (Messiah 1962), is

$$Y_{L'}(\hat{r}) h_{L'}^{(\pm)}(\kappa r) = \sum_{L_1, L_2} i^{l_1+l_2-L'} (-1)^{m'} F_{m_1, m_2, -m'}^{l_1, l_2, L'} Y_{L_1}(\hat{r}_n) Y_{L_2}(\hat{R}_n) h_{l_1}^{(\pm)}(\kappa r_n) j_{l_2}(\kappa R_n) \quad (2)$$

where $\vec{r}_n = \vec{r} - \vec{R}_n$ and

$$F_{m_1, m_2, m_3}^{l_1, l_2, l_3} = [4\pi(2l_1+1)(2l_2+1)(2l_3+1)]^{\frac{1}{2}} \begin{pmatrix} l_1 & l_2 & l_3 \\ 0 & 0 & 0 \end{pmatrix} \begin{pmatrix} l_1 & l_2 & l_3 \\ m_1 & m_2 & m_3 \end{pmatrix}. \quad (3)$$

$\begin{pmatrix} l_1 & l_2 & l_3 \\ m_1 & m_2 & m_3 \end{pmatrix}$ is the Wigner 3-j symbol.

It follows that the incident wave on each scatterer is:

$$\psi_i(\vec{r}_n) = \sum_{L'} Y_{L'}(\hat{r}_n) j_{L'}(\kappa r_n) g_{nL'}^0 \quad (4)$$

where

$$g_{nL_1}^0 = \sum_L M_{L_1 L}^n f_L^0 \quad (5)$$

or, in matrix form

$$\mathbf{g}^0 = \mathbf{M} \mathbf{1} \cdot \mathbf{f}^0 \quad (6)$$

with

$$M_{L_1 L}^n = \sum_{L_2} i^{l_1+l_2-L} (-1)^m F_{m_1, m_2, -m}^{l_1, l_2, L} Y_{L_2}(\hat{R}_n) j_{l_2}(\kappa R_n). \quad (7)$$

We can now incorporate the multiple scattering between the two scatterers to obtain a global expression for the total impinging wave on each molecule. This has the form

$$\psi_i(\vec{r}_n) = \sum_L Y_L(\hat{r}_n) j_l(\kappa r_n) g_{nL}. \quad (8)$$

One can identify our g_{nL} with the expression $4\pi i^l e^{i\vec{k} \cdot \vec{R}_n} B_{\vec{k}L}^{(n)}$ in the analysis of Caron & Sanche (2004). By comparing Eq. (8) to the total impinging part of their Eq. (1), *i.e.* the first term on the right-hand side, one then gets from their Eq. (2)

$$\begin{aligned}
g_{nL} &= g_{nL}^0 + \frac{1}{2} \sum_{L_1, L_2, L'_2} i^{l_1+l-l'_2} T_{L'_2 L_2}^{n'} g_{n' L_2} (-1)^{m'_2} F_{m_1, m_2, -m'_2}^{l_1, l, l'_2} Y_{L_1}(\hat{R}_{nn'}) h_{l_1}^+(\kappa R_{nn'}) \\
&= g_{nL}^0 + \sum_{L_2 L'_2} \chi_{LL'_2}^{nn'} T_{L'_2 L_2}^{n'} g_{n' L_2}
\end{aligned} \tag{9}$$

with $\vec{R}_{nn'} = \vec{R}_n - \vec{R}_{n'}$, $n' = -n$.

$$\chi_{LL'_2}^{nn'} = \frac{1}{2} \sum_{L_1} i^{l_1+l-l'_2} (-1)^{m'_2} F_{m_1, m_2, -m'_2}^{l_1, l, l'_2} Y_{L_1}(\hat{R}_{nn'}) h_{l_1}^+(\kappa R_{nn'}) \tag{10}$$

expresses how a scatterer influences its neighbour. Note that for $n = n'$ $\chi_{LL'}^{nn} = 0$. The second term on the right side of (9) is the total scattered wave from the second scatterer n' . In matrix form, (9) can be written as

$$\mathbf{g} = (\mathbf{I} - \chi \mathbf{T})^{-1} \cdot \mathbf{g}^0. \tag{11}$$

Now, we have to combine the amplitudes scattered from each scatterer

$$\psi_s(\vec{r}) = \sum_n \psi_s(\vec{r}_n) = \sum_n \sum_{LL'} Y_{L'}(\hat{r}_n) \frac{1}{2} h_{l'}^{(+)}(\kappa r_n) T_{L'L}^n g_{nL}. \tag{12}$$

around the common origin (centre of mass) using

$$Y_{L'}(\hat{r}_n) h_{l'}^{(\pm)}(\kappa r_n) = \sum_{L_1, L_2} i^{l_1+l_2-l'} (-1)^{m'} F_{m_1, m_2, -m'}^{l_1, l_2, l'} Y_{L_1}(\hat{r}) Y_{L_2}(-\hat{R}_n) h_{l_1}^{(\pm)}(\kappa r) j_{l_2}(\kappa R_n). \tag{13}$$

One gets

$$\psi_s(\vec{r}) = \sum_{L_1} Y_{L_1}(\hat{r}) \frac{1}{2} h_{l_1}^{(+)}(\kappa r) \sum_{n, L, L'} M2_{L_1 L'}^n T_{L'L}^n g_{nL} \tag{14}$$

where

$$M2_{L_1 L'}^n = \sum_{L', L_2} i^{l_1+l_2-l'} (-1)^{m'} F_{m_1, m_2, -m'}^{l_1, l_2, l'} Y_{L_2}(-\hat{R}_n) j_{l_2}(\kappa R_n). \tag{15}$$

Combining (14), (6), (11) and referring to the general expression (1), we have

$$\mathbf{T}^{tot} = \mathbf{M2} \cdot \mathbf{T} \cdot (\mathbf{I} - \chi \mathbf{T})^{-1} \cdot \mathbf{M1}. \tag{16}$$

We thus obtain the T-matrix for two identical scatterers from their individual T-matrices. **M1** and **M2** account for the transformation from the monomer to the dimer's centre of mass and $(\mathbf{I} - \chi \mathbf{T})^{-1}$ expresses the multiple scattering between the two scatterers.

3. Characteristics of the calculations

No experimental or theoretical data on elastic LEE collisions with the water dimer are available. Therefore, in order to test the quality of our MS results, we have performed an *ab initio* scattering calculation on the gas-phase dimer using the R-matrix method and the UK polyatomic R-matrix suite (Morgan et al. 1998).

The gas-phase water dimer in its ground state equilibrium geometry has C_s symmetry (Figure 1). The geometry parameters from Park C-Y et al. (2001) were used in the R-matrix calculation. The geometry of the water monomer is very slightly changed upon dimer

formation (see Table 1). In the MS calculation, the dimer was formed by putting together two water molecules separated by $d \sim 5.5$ bohr along the Z-axis. This means that there are very minor differences between the geometries used in the R-matrix and MS calculations. The most notable is the hydrogen bond r_{OH} which is at most ~ 0.013 bohr longer in the dimer than in the monomers we use to build the MS results.

3.1. R-matrix calculation for the dimer

A detailed description of the R-matrix method as applied to polyatomic molecules within the fixed-nuclei (FN) approximation can be found in Morgan et al. (1997) and Morgan et al. (1998). The method is based on splitting coordinate space into two regions separated by a sphere, henceforth called R-sphere, centred on the centre of mass of the molecule. The radius of the R-sphere is chosen in such way that the electronic density of the target is negligible outside it. As a consequence, exchange and correlation effects can be neglected in this outer region and a long-range multipole expansion used to represent the electron-target interaction. Inside the R-sphere, both effects are significant and are therefore taken into account using rigorous quantum chemistry methods. The wavefunction for the target + electron system is then expressed in terms of a close-coupling expansion.

The calculation was performed following previous work on electron scattering from isolated H_2O (Gorfinkiel et al. 2002). We used the equilibrium geometry from Park C-Y et al. (2001) and the same basis set (including the diffuse functions) employed for the monomer work by Gorfinkiel et al. (2002). Since in this work we are concerned with the elastic scattering, only the ground electronic state was considered and included in the close-coupling expansion. We therefore produced natural orbitals exclusively from this state and then used them in a CASCI (complete active space configuration interaction) calculation in which 8 electrons are frozen; this generated around 7000 configurations. With this model, we obtained a good value for the ground state energy: -152.18 hartree, compared to -152.67 hartree from the most accurate calculation. We also obtained excellent agreement with the experimental dipole moment: 1.065 a.u. in our calculations compared to 1.041 a.u..

We used an R-sphere radius of $a=13$ bohr. In order to confirm that all the electronic density was contained inside the sphere, tests were performed for radii of $a=14$ and $a=15$ bohr. Only small differences at very low energies were found between the cross sections calculated with the three radii (Gorfinkiel 2008). The continuum orbitals describing the scattered electron were expanded in a basis of GTOs with $l \leq 4$ centred on the centre of mass of the water molecule.

3.2. Multiple scattering calculation

In I, we showed that gas-phase R-matrix data can be efficiently used in conjunction with MS theory in a non-gaseous environment by deriving the band structure of a molecular crystal (ice). The fundamental lesson learnt from this KKR study is that for the multiple scattering term, we need a trimmed T matrix T_c , without dipole contribution for radii $r > a_c$ and with an angular momentum cut-off. Thus two different monomer T-matrices are needed: T_c for

the multiple scattering term $(\mathbf{I} - \chi \mathbf{T}_c)^{-1}$ and a matrix \mathbf{T}_{dip} for which no cut-offs are applied. With this in mind Eq. 16 can be rewritten:

$$\mathbf{T} = \mathbf{M2} \cdot \mathbf{T}_{\text{dip}} \cdot (\mathbf{I} - \chi \mathbf{T}_c)^{-1} \cdot \mathbf{M1} . \quad (17)$$

The first step in our multiple scattering calculation involves generating the monomer T-matrices \mathbf{T}_c and \mathbf{T}_{dip} required in equation (17). The description of LEE scattering by an isolated H_2O molecule is the same than in I. Since a detailed description of the calculation was given there, we will limit ourselves here to a brief summary. We have used the R-matrix method within the fixed-nuclei approximation. For the target description we used the DZP basis set (Dunning 1970) for the Oxygen and a TZ basis (Dunning 1971) for the Hydrogen. A CASCI model was used with only 2 frozen electrons and the calculation included only the ground state. The scattering calculation was performed with an R-sphere radius of $a = 6$ bohr. A GTO basis for the continuum with $l \leq 4$ was generated for this radius using the program GTOBAS (Faure et al. 2002) . The obtained T-matrices were rotated from the R-matrix coordinates to their corresponding position in the dimer. The procedure to do so was explained previously (Equation (24) in I) and the reader is referred to that work for further details.

As mentioned above, two cut-offs are applied when generating \mathbf{T}_c . A first cut-off on the range of the molecular dipole is achieved by removing the dipole field for $r > a_c$. The cut-off radius a_c depends only on the dipole moment of the molecular monomer and should therefore be the same for the ice and the dimer calculations. In I, we have found that $a_c \sim 6.5$ bohr yields the best value for the electron's effective mass in ice. An analysis of the electron-(isolated) water cross section obtained for different values of a_c supports this finding (the reader is referred to Fig. 1 in I): for too small cut-off radii ($a_c < 6$), the high energy cross section is unphysical whereas for higher radii ($a_c > 6$) the cross section exhibits a dipole-driven behaviour (it increases rapidly at low energy). Although this behaviour is physical and should be expected, it is the aim of the cut-off to at least partially eliminate it. This can be understood as an attempt to ensure that \mathbf{T}_c involves only the contribution of the target potential in the small region around the scatterer. That leaves $a_c \sim 6$ bohr as the most satisfactory radius.

The second cut-off, in the angular momentum components l of the scattering matrix, is critical and depends both on the electron kinetic energy E and the intermolecular distance d . The restriction is related to the angular momentum energy barrier $E(l, r) = l(l + 1)/r^2$. The KKR calculation predicts that only angular momentum values $l \leq l_c$ should be retained such that $E(l_c, d) < E_e < E(l_c + 1, d)$ with $E(l, d) = l(l + 1)/d^2$ Ry. That is, only electrons that scatter from one monomer with energy larger than $E(l, d)$ can reach the other one and undergo multiple scattering. In the dimer, the two H_2O molecules are separated by $d \sim 5.5$ bohr (almost the same intermolecular distance than in crystalline ice in I). We expect then to have the same cut-off criteria than in the KKR calculation.

Once the T-matrices for the monomer are calculated, the dimer T-matrix in equation 17 is built. From it, we build the R-matrix at $r = a_{\text{dip}} = 9$ bohr using the approach given in Appendix A and propagate it outwards (Baluja et al. 1982) using *the exact dipolar field of the dimer*. This is necessary in order to incorporate the effect of the dipole moment of the dimer

in the MS description. To choose a_{dip} we propagate the R-matrix of the dimer (obtained with the R-matrix calculation) inwards from the asymptotic region and then calculate the CS from it. The low-energy part of this CS decreases the more of the dipole field we remove (the further in we go) and takes an unsuspected and incorrect upturn for a radial distance of 9 bohr. We believe that for this distance the multipolar field of the dimer is no longer describable by its total dipole field. We finally generate the final T-matrix \mathbf{T}^{tot} which takes the dimer's dipole contribution into account. This T-matrix is a function of energy and of the angular momentum cut-off l_c used for \mathbf{T}_c in the multiple scattering term of Eq. 17. The integral elastic cross section is then obtained using the well known formula:

$$\sigma(E) = \frac{\pi}{k^2} \sum_{l'} |T_{l'}^{tot}|^2 \quad (18)$$

In Figure 2, we present the CS for different l_c values. As mentioned earlier, the partial wave expansion must be limited as the collision energy decreases. For example, for electron energies between $5.4 < E < 9$ eV, the KKR calculation predicts that we can only include $l \leq 3$ in the MS calculation. It can be easily seen from Figure 2, that the CS is ill behaved in this region (below ~ 7 eV) when $l_c = 4$. A closer look at the CS for the other values of l_c shows the presence of a critical energy below which the CS does not exhibit the right behaviour. These critical energies are at slightly lower energies than the value given by $E(l_c, d)$.

If we scrupulously restrict the calculation to integer values of l_c for electron energies between $E(l_c, d)$ and $E(l_c + 1, d)$, the CS will be jagged *i.e.* discontinuous at $E(l_c, d)$. Smoothing is needed. A two-point interpolation on the parameter l between l_c and $l_c + 1$, where l is the solution of $E = l(l + 1)/d^2$, would get rid of the discontinuities. But this would admix the CS at l_c with any singular part of the CS at $l_c + 1$. A quick look at Figure 2 indicates, for instance, that at 6 eV when $l_c = 3$ the interpolation would spuriously bring in a sizable part of the huge peak of the $l_c = 4$ CS. The procedure can be regularised by upward shifting $E(l_c, d)$ using a parameter γ such that $\gamma E_s(l_c, d) = l_c(l_c + 1)/d^2$. A value of $\gamma = 0.75$ would shift the cut-off energies to the new values shown in Figure 2, beyond the threshold of the singular behaviour of the CS for $l_c + 1$. The interpolation procedure can now be done safely with l a solution of $\gamma E_s = l(l + 1)/d^2$. The CS is linearly interpolated between CS values corresponding to the closest lower and larger integer values of l .

4. Results

The elastic electron-(H₂O)₂ cross section versus impact energy is plotted in Figure 3. As a test of the accuracy of the MS calculation, we compare our results to the CS calculated with the R-matrix codes. The agreement between the two calculation is very good. The multiple scattering cross section is slightly higher than the R-matrix one but remains within 5% of the the fully *ab initio* CS for energies larger than 2.5 eV. We believe these differences are well within the range of usual experimental errors and *ab initio* calculation uncertainties. For targets with large dipole moments, it is customary to add to the R-matrix cross section a Born based correction (Chu & Dalgarno 1974) to account for the partial waves not included in the

ab initio calculation. This correction is the same for the R-matrix and MS calculations and for this reason has not been included in the cross sections plotted in Figure 3.

Based on the results of I, the need for a “trimmed” T-matrix (\mathbf{T}_c) in the MS term of (17) is obvious. Figure 2 illustrates the drastic impact of a larger angular momentum basis; including higher l at low energies introduces resonances and/or premature divergences in the CS caused by the resonant nature of the MS $(\mathbf{I} - \chi\mathbf{T})^{-1}$ term in Eq. 17. The cut-off in the long-range dipolar interaction is also very important. In I, we have shown that even though the value of the cut-off a_c is not critical for band structure calculations, a too large or too small cut-off radius has a noticeable effect on the value of the effective mass (which was used for calibration purposes). The two cut-offs are necessary and have to be applied only to the MS term. The use of a full T-matrix \mathbf{T}_{dip} in (17) is, however, essential to get the right CS behaviour at low energies and to properly account for the potential produced by the dipole of a H_2O molecule. The need for \mathbf{T}_{dip} to include the dipole contribution arises from the fact that for $r \leq a_{\text{dip}}$, the scattering electron feels the individual dipoles of the isolated water molecules.

The radius a_{dip} has to be chosen in a proper way. It must allow the separation between the regions where the individual water dipoles dominate the electron-molecule interaction ($r < a_{\text{dip}}$) and the region where the total dipole of the dimer dominates ($r > a_{\text{dip}}$). Based on a geometrical analysis (Figure 4), one can see that a radius of 9 bohr is an adequate choice. In order to check the appropriateness of this value, we have tried several R-sphere radii ranging from 6 to 13 bohr and confirmed that 9 bohr yields the best cross section.

It is evident from Figure 4, that a choice of $a \simeq a_c \simeq 6$ bohr in our calculations does not exactly correspond to a non-overlapping potentials picture. For the spheres not to overlap we would need a radius around $d/2 \simeq 2.7$ bohr. However, using such small radius does not provide a good representation of the target. This was already clear in I, where we established that small radii introduce a discontinuity at the boundary of the sphere that is too important to lead to good results.

5. Conclusions and Discussion

We have developed a technique to derive the total T-matrix of two scatterers from their individual T-matrices as described by Eq. (16). The technique first involves finding the T-matrix describing the scattering for an isolated molecular target. These are then combined using Eq. 17. Our main conclusion is that two different T-matrices, with different constraints, are needed to represent the electron-dimer interaction: two cut-offs have to be applied only to the MS term (\mathbf{T}_c but not \mathbf{T}_{dip}). From the total T-matrix, the R-matrix at a_{dip} is determined and then propagated to an asymptotic distance using the dipole moment of the cluster. This propagation is fundamental in order to incorporate the electron interaction with the true dimer dipole moment. One can argue that the need for \mathbf{T}_{dip} and a_{dip} is a surface effect not present in the infinite crystal situation in I. In fact, the dimer is mostly surface.

Our results show that a multiple scattering calculation can efficiently replace a *standard ab initio* scattering calculation for this system. Very good agreement is found between the MS

and the R-matrix cross sections. The MS method should allow us to calculate elastic cross sections for small water clusters that are nevertheless too big to be studied *ab initio*. The same value of a_c should be employed and a_{dip} could be determined using the same geometrical considerations. How large a cluster could one attempt to treat using this procedure? The cluster should have a large surface to volume ratio. The arguments presented in Appendix B indicate that the number of water molecules should be much less than 500. That leaves a lot of room for fair sized clusters.

For very large clusters, having a low surface to volume ratio, the general picture would be as follows. The physical space should be divided into three parts. In the innermost part, the bulk of the cluster, MS theory using \mathbf{T}_c in a uniform background optical potential U_{op} , measuring the average polarisation potential energy between the muffins, would be used as in I. Note that the resonant MS $(\mathbf{I} - \chi\mathbf{T}_c)^{-1}$ term of Eq. (17), which has been freed of any spurious peaks through the angular momentum cut-off algorithm, will yet show peaks that correspond to damped electronic modes of the cluster. These are, for instance, the modes that were calculated for crystalline ice in I. Then there would be a narrow surface region which adapts the bulk value of the optical potential to the vacuum level and in which \mathbf{T}_c would be used for the MS part and \mathbf{T}_{dip} for the exit part. Finally, there would be an outer region in which the R-matrix of the two inner regions can be propagated to infinity using the multipolar potential of the cluster.

We have thus far discussed only elastic scattering. How can one deal with inelastic collisions? Although this is uncharted territory, the scenario will likely go as follows. In such a situation, new energy channels open up. For each of these, there will be energy-diagonal T-matrices $T_d(E_i)$ and cross-energy ones $T_{nd}(E_i, E_j)$. These will combine into a super-matrix $T(E_i, E_j) = T_d(E_i)\delta_{E_i, E_j} + T_{nd}(E_i, E_j)$. The rest would basically be a repeat of what we have done for a single channel. One would define the MS part \mathbf{T}_c with cut-offs on the range of the dipole and on the angular momentum basis. Note that the latter is different for each energy channel. Moreover, as the energy increases, larger and larger angular momenta will be needed. Some adjustments on a_c might also be required in order to include inelastic channels involving more extended molecular wavefunctions. Formally, Eq. (17) still applies to these super matrices. The resonant MS $(\mathbf{I} - \chi\mathbf{T}_c)^{-1}$ term would not only exhibit peaks related to the damped electronic modes of the cluster but also structures caused by the inelastic contributions to \mathbf{T}_c which will in turn modulate the inelastic peaks in \mathbf{T}_{dip} . Interpolation of the total CS would now involve linear interpolation of the type described above in a multi-dimensional energy-channel space. The computer time consuming aspect comes from repeated cluster calculations of Eq. (17) for many values of the incoming electron energy E_i and $l_c(E_i)$.

Acknowledgments

This research is supported by the Canadian Institutes of Health Research and the EPSRC.

Appendix A. Relation between \mathbf{R} and \mathbf{K} matrices

We suppose in the following, that the \mathbf{R} -matrix defined at a radius $r = a$ describes the inner region $r \leq a$ and that the potential outside the sphere is zero. For elastic scattering we have (Burke & Berrington 1993),

$$F_L(a) = \sum_{L'} R_{LL'} \left[r \frac{d}{dr} F_{L'} \right]_{r=a} . \quad (\text{A.1})$$

with F_L the reduced radial wavefunctions.

For $r > a$, the wavefunction representing the scattering electron is

$$\psi(\vec{r}) = \sum_L \frac{F_L(r)}{r} Y_L(\hat{r}) . \quad (\text{A.2})$$

In the region $r > a$, one can write

$$F_L(r) = f_{1L} \bar{j}_\ell(\kappa r) + f_{2L} \bar{\eta}_\ell(\kappa r) \quad (\text{A.3})$$

where $\bar{j}(z) = z j(z)$ and $\bar{\eta}(z) = z \eta(z)$. $F_L(r)$ is a solution of energy $E = \kappa^2/2$ and angular momentum L of the Schrödinger equation in a zero potential. Substituting (A.3) in (A.1), we have

$$f_{1L} \bar{j}'_\ell(\kappa a) + f_{2L} \bar{\eta}'_\ell(\kappa a) = a\kappa \sum_{L'} R_{LL'} [f_{1L'} \bar{j}'_{\ell'}(\kappa a) + f_{2L'} \bar{\eta}'_{\ell'}(\kappa a)] , \quad (\text{A.4})$$

where $\bar{j}'_\ell(z) = d\bar{j}_\ell(z)/dz$ and $\bar{\eta}'_\ell(z) = d\bar{\eta}_\ell(z)/dz$. One can rearrange this equation and write it in matrix form

$$\left(\bar{\mathbf{N}} - a\kappa \mathbf{R} \bar{\mathbf{N}}' \right) f_2 = - \left(\bar{\mathbf{J}} - a\kappa \mathbf{R} \bar{\mathbf{J}}' \right) f_1 \quad (\text{A.5})$$

where $\bar{J}_{LL'} = \bar{j}_\ell(\kappa a) \delta_{LL'}$, $\bar{N}_{LL'} = \bar{\eta}_\ell(\kappa a) \delta_{LL'}$ and f_1, f_2 are the amplitude column vectors. This gives us:

$$f_2 = - \left(\bar{\mathbf{N}} - a\kappa \mathbf{R} \bar{\mathbf{N}}' \right)^{-1} \left(\bar{\mathbf{J}} - a\kappa \mathbf{R} \bar{\mathbf{J}}' \right) f_1 \quad (\text{A.6})$$

We introduce the \mathbf{K} -matrix,

$$\mathbf{K} = \left(\bar{\mathbf{N}} - a\kappa \mathbf{R} \bar{\mathbf{N}}' \right)^{-1} \left(\bar{\mathbf{J}} - a\kappa \mathbf{R} \bar{\mathbf{J}}' \right) . \quad (\text{A.7})$$

Substituting (A.7) in (A.6) and then in (A.3) and (A.2), we have for $r > a$

$$\psi(\vec{r}) = (\kappa r)^{-1} \sum_{LL'} f_{1L} [\bar{j}_\ell(\kappa r) \delta_{LL'} - K_{L'L} \bar{\eta}_\ell(\kappa r)] Y_{L'}(\hat{r}) \quad (\text{A.8})$$

and thus

$$\lim_{r \rightarrow \infty} \psi(\vec{r}) = (\kappa r)^{-1} \sum_{LL'} f_{1L} [\sin(\kappa r - \ell\pi/2) \delta_{LL'} + K_{L'L} \cos(\kappa r - \ell'\pi/2)] Y_{L'}(\hat{r}) , \quad (\text{A.9})$$

which is conform to the definition of the \mathbf{K} matrix.

Eq. (A.7) gives a 'passage' for the transformation $\mathbf{R} \leftrightarrow \mathbf{K}$. It is worth noting that the \mathbf{R} -matrix depends on the radius but not the \mathbf{K} -matrix (nor the transmission matrix \mathbf{T} , or the scattering matrix \mathbf{S}). So once we have the \mathbf{R} -matrix for any radius a we can build the \mathbf{K} -matrix using Eq. (A.7) and inversely. The \mathbf{T} -matrix is then obtained from the \mathbf{K} -matrix using the well known relation:

$$\mathbf{T} = 2i\mathbf{K}(1 - i\mathbf{K})^{-1} \quad (\text{A.10})$$

Appendix B. Surface to volume ratio

One can estimate a surface to volume ratio by the ratio of the number of surface molecules N_s to the number of bulk molecules N_b . One can get an estimate of these numbers by considering a spherical cluster of radius R_c . The surface molecules are located in the shell between R_c and $R_c - d$ where d is, as above, the distance between molecules. If the mid-shell surface area $S = 4\pi(R_c - d/2)^2$ is occupied by molecules forming a close packed array, the area occupied by one molecule would be $S_{mol} \approx d^2\sqrt{3}/2$ and thus $N_s = S/S_{mol}$. Assuming the bulk of volume $V = 4\pi(R_c - d)^3/3$ is occupied by close packed molecules occupying a volume of $V_b = 0.93d^3\sqrt{3}/2$, one gets $N_v = V/V_b$. A high surface to volume ratio can thus be quantised by the quantity $SV = N_s/N_b \gg 1$. With $d = 5.5$ a.u. one gets $R_c \ll 4.6$. One thus deduces that the cluster must contain much less than $N_s + N_v \approx 500$ molecules to have a large surface to volume ratio.

References

- Baluja K L, Burke P G & Morgan L A 1982 *Comput. Phys. Commun.* **27**, 299.
 Barnett R, Landman U & Nitzan A 1989 *J. Chem. Phys.* **91**, 5567.
 Becker D, Sevilla M D, Wang W & LaVere T 1997 *Radiat. Res.* **148**, 481.
 Belić D S, Landau M & Hall R I 1981 *J. Phys. B: At. Mol. Phys.* **14**, 175.
 Burke P G & Berrington K A 1993 Institute of Physics Publishing Bristol and Philadelphia.
 Caron L G, Bouchiha D, Gorfinkiel J D & Sanche L 2007 *Phys. Rev. A* **76**, 032716.
 Caron L G & Sanche L 2003 *Phys. Rev. Lett.* **91**, 113201.
 Caron L G & Sanche L 2004 *Phys. Rev. A* **70**, 032719.
 Caron L G & Sanche L 2005 *Phys. Rev. A* **72**, 032726.
 Chu S I & Dalgarno A 1974 *Phys. Rev. A* **10**, 788.
 Compton R N & Christophorou L G 1967 *Phys. Rev.* **154**, 110.
 Curtis M G & Walker I C 1992 *J. Chem. Soc., Faraday Trans.* **88**, 2805.
 Dill D & Dehmer J L 1974 *J. Chem. Phys.* **61**, 692.
 Dunning T H 1970 *J. Chem. Phys.* **53**, 2823.
 Dunning T H 1971 *J. Chem. Phys.* **55**, 716.
 Faure A, Gorfinkiel J D, Morgan L A & Tennyson J 2002 *Computer Phys. Commun.* **144**, 224–241.
 Fedor J, Cicman P, Coupier B, Feil S, Winkler M, Gluch K, Husarik J, Jaksch D, Farizon B, Mason N J, Scheier P & Märk T D 2006 *J. Phys. B: At. Mol. Phys.* **39**, 3935.
 Garrett B C, Dixon D A, Camaioni D M, Chipman D M, Johnson M A, Jonah C D, Kimmel G A, Miller J H, Rescigno T N, Rossky P J, Xantheas S S, Colson S D, Laufer A H, Ray D, Barbara P F, Bartels D M, Becker K H, Bowen K H, Bradforth S E, Carmichael I, Coe J V, Corrales L R, Cowin J P, Dupuis M, Eienthal K B, Franz J A, Gutowski M S, Jordan K D, Kay B D, LaVerne J A, Lyman S V, Madey T E, McCurdy C W, Meisel D, Mukamel S, Nilsson A R, Orlando T M, Petrik N G, Pimblott S M, Rustad J R, Schenter G K, Singer S J, Tokmakoff A, Wang L-S, Wettig C & Zwiernik T S 2005 *Chem. Rev.* **105**, 355.
 Gil T J, Rescigno T N, McCurdy C W & III B H L 1994 *Phys. Rev. A* **49**, 2642.
 Gorfinkiel J D 2008 in preparation.
 Gorfinkiel J D, Morgan L A & Tennyson J 2002 *J. Phys. B* **35**, 543.
 Haxton D J, McCurdy C W & Rescigno T N 2007 *Phys. Rev. A* **75**, 012711.
 Herring-Captain J, Grieve G A, Alexandrov A, Sieger M T, Chen H & Orlando T M 2005 *Phys. Rev. B* **72**, 035431.
 Itikawa Y & Mason N J 2005 *J. Phys. Chem. Ref. Data* **34**, 1.
 Knapp M, Echt O, Kreisler D & Recknagel E 1986 *J. Chem. Phys.* **85**, 636.

- Knapp M, Echt O, Kreisle D & Recknagel E 1987 *J. Phys. Chem.* **91**, 2601.
- Lee G H, Arnold S T, Eaton J G, Sarkas H W, Bowen K H, Ludewigt C & Haberland H 1991 *Z. Phys. D* **20**, 9.
- Lozier W N 1930 *Phys. Rev.* **36**, 1417.
- Messiah A 1962 *Quantum Mechanics* Wiley New York.
- Michaud M, Wen A & Sanche L 2003 *Radiat. Res.* **159**, 3.
- Morgan L A 1998 *J. Phys. B* **31**, 5003.
- Morgan L A, Gillan C J, Tennyson J & Chen X 1997 *J. Phys. B: At. Mol. Phys.* **30**, 4087.
- Morgan L A, Tennyson J & Gillan C J 1998 *Computer Phys. Commun.* **114**, 120.
- Park C-Y, Kim Y & Kim Y 2001 *J. Chem. Phys.* **115**, 2926.
- Ptasinska S & Sanche L 2007 *Phys. Rev. E* **75**, 031915.
- Rawat P, Prabhudesai V S, Aravind G, Rahman M A & Krishnakumar E 2007 *J. Phys. B: At. Mol. Phys.* **40**, 4625–4636.
- Rowntree P, Parenteau L & Sanche L 1991 *J. Chem. Phys.* **94**, 8570.
- Sanche L & Schulz G J 1972 *J. Chem. Phys.* **58**, 479.
- Schulz G J 1960 *J. Chem. Phys.* **33**, 1661.
- Simpson W C, Sieger M T, Orlando T M, Parenteau L, Nagesha K & Sanche L 1997 *J. Chem. Phys.* **107**, 8668.
- Valenzano L, van Hemert M C & Kroes G J 2005 *The Journal of Chemical Physics* **123**, 034303.
- Weber J M, Leber E, Ruf M W & Hotop H 1999 *Eur. Phys. J. D* **7**, 587.

Tables and table captions

| | H ₂ O | (H ₂ O) ₂ |
|-------------------|------------------|---------------------------------|
| r_{OH1} | 1.81 | 1.810 |
| r_{OH2} | 1.81 | 1.823 |
| θ_1 | 104.5 | 104.5 |
| $r_{OH3}=r_{OH4}$ | | 1.814 |
| r_{OO} | | 5.497 |
| θ_2 | | 104.6 |
| α | | 4.7 |
| β | | 55.1 |

Table 1. H₂O and (H₂O)₂ geometries used in our calculations. The values of the dimer parameters (see figure 1 for identification) are from Park C-Y et al. (2001). Length units are in bohr and angles in deg.

Figure captions

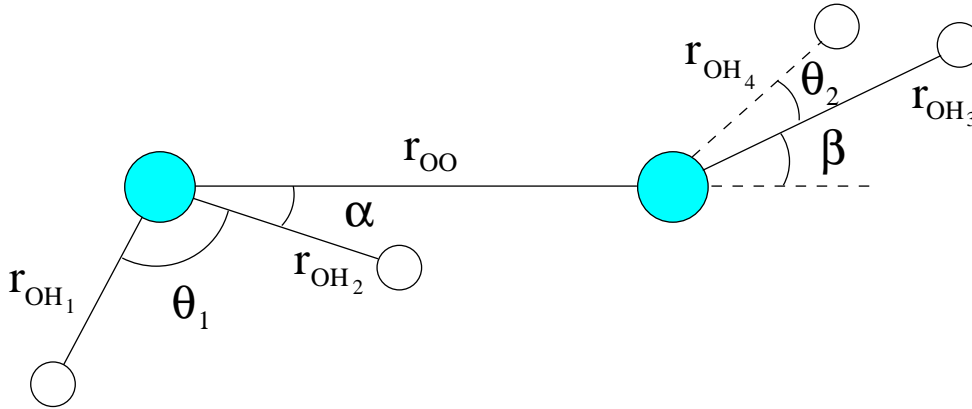


Figure 1. Ground state equilibrium geometry of $(\text{H}_2\text{O})_2$. The parameters' values are listed in Table 1.

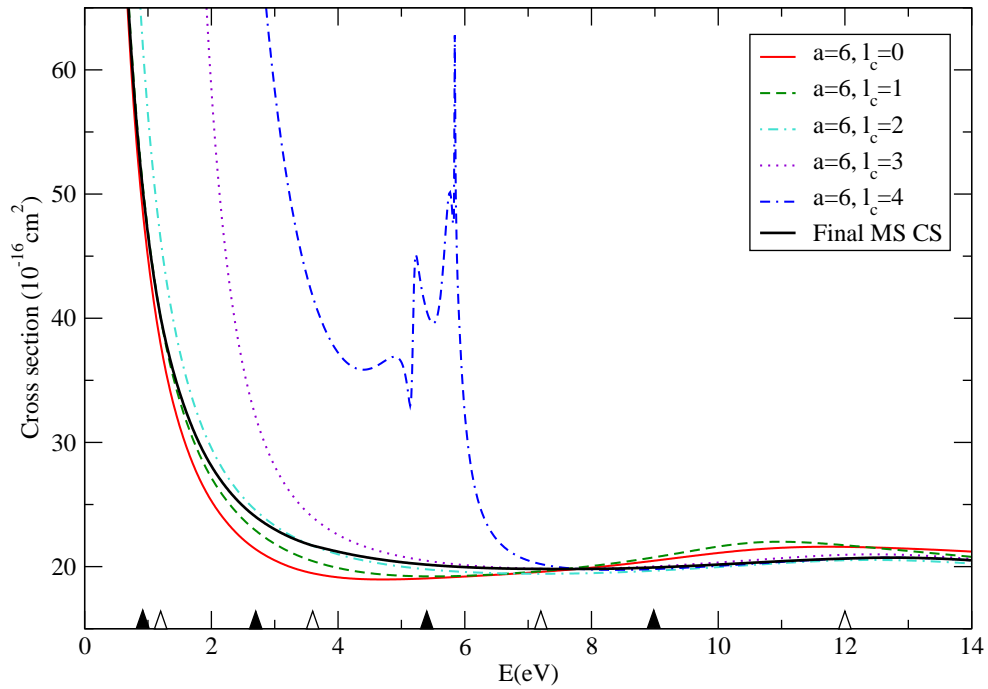


Figure 2. Trial elastic electron-water dimer cross sections calculated using different angular momentum cut-offs l_c . The MS term in Eq. (17) introduces unphysical resonances and/or premature divergences in the CS. The filled arrowheads point to the cut-off energies $E(l_c, d)$ while the empty arrowheads point to the shifted regularised energies $E_s(l_c, d)$ for $l_c = 1, 2, 3, 4$ respectively, from left to right.

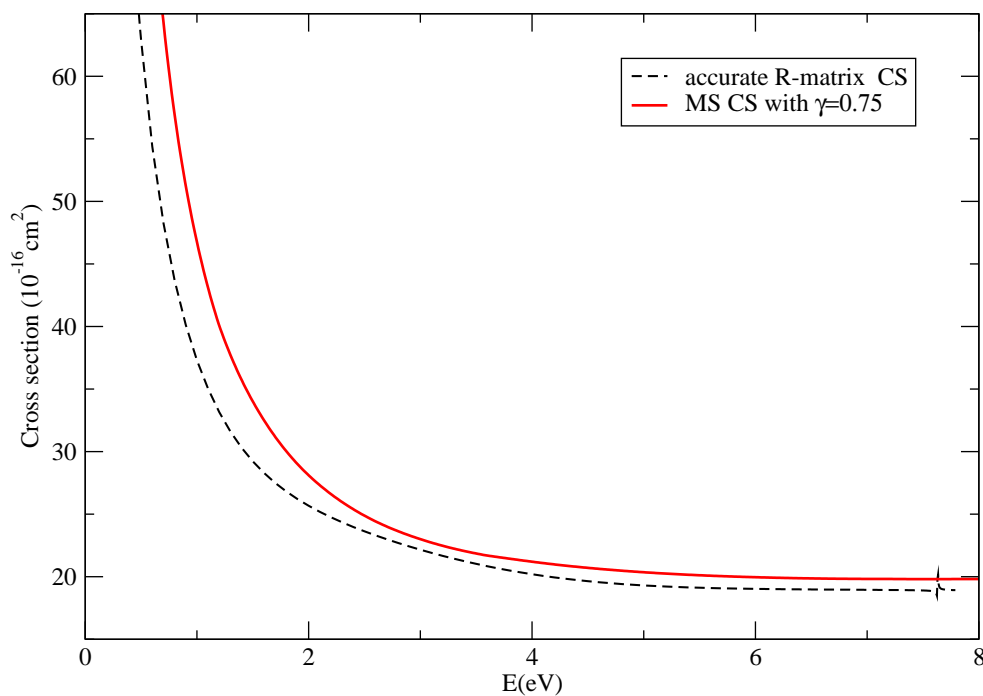


Figure 3. Elastic electron-(H₂O)₂ cross sections. The MS cross section was obtained following the smoothing prescription explained in the text. Notice that the first vertical excitation threshold is located around 6.99 eV (Valenzano et al. 2005).

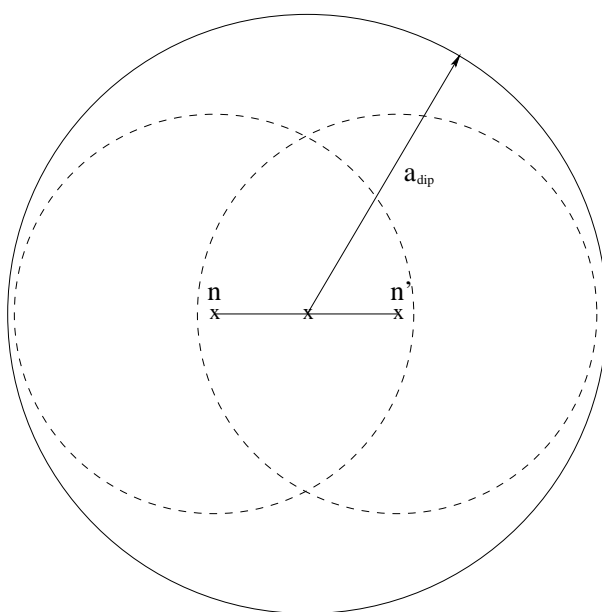


Figure 4. Radii used in the MS calculations; solid line: $a_{dip} = 9$ bohr, for inclusion of the dimer's dipole effect. Dashed line: R-sphere with radius $a = 6$ bohr used in the R-matrix calculation for the monomer. n and n' define the positions of the centre of mass of each water molecule.